Nanoscale

The use of advanced spectral imaging to reveal nanoparticle identity in the biological samples

Journal:	*Nanoscale*
Manuscript ID	NR-COM-11-2021-007551.R1
Article Type:	Communication
Date Submitted by the Author:	27-Dec-2021
Complete List of Authors:	Alshammari, Qamar; Chapman University College Pala, Rajasekharreddy; CSIR-Indian Institute of Chemical Technology, Biology and Biotechnology; Chapman University, Pharmacy Barui, Ayan Kumar; Chapman University College Alshammari, Saud; Chapman University College Nauli, Andromeda; Chapman University, Pharmacy Katzir, Nir; Spectral Imaging, Inc. Mohieldin, Ashraf; Chapman University College Nauli, Surya; Chapman University College,

The use of advanced spectral imaging to reveal nanoparticle identity in the biological samples

Qamar A. Alshammari[*,1,2], Rajasekharreddy Pala[*,1], Ayan K. Barui[1], Saud O. Alshammari[1,3], Andromeda M Nauli[4], Nir Katzir[5], Ashraf M. Mohieldin[1], and Surya M. Nauli[1,6]

[*]Authors contribute equally
[1]Department of Biomedical & Pharmaceutical Sciences, Harry and Diane Rinker Health Science Campus, Chapman University, 9401 Jeronimo Road, Irvine, CA 92618-1908, USA
[2]Department of Pharmacology and Toxicology, Faculty of Pharmacy, Northern Border University, KSA.
[3]Department of Plant Chemistry and Natural Products, Faculty of Pharmacy, Northern Border University, KSA
[4]Department of Pharmaceutical Sciences, College of Pharmacy, Marshall B. Ketchum University, Fullerton, CA, USA.
[5]Applied Spectral Imaging, 5315 Avenida Encinas, Suite 150, Carlsbad, CA 92008.
[6]Department of Medicine, University of California Irvine, Irvine, CA 92868, USA.

Corresponding author:
Surya M. Nauli
Chapman University
University of California Irvine
9401 Jeronimo Road.
Irvine, CA 92618-1908
Tel: 714-516-5480
Fax: 714-516-5481
Email: nauli@chapman.edu; snauli@uci.edu

Abstract

Metal nanoparticles (NPs) have been used in drug delivery therapy, medical diagnostic strategy, and the current Covid-19 vaccine carriers. Many microscope-based imaging systems have been introduced to facilitate detection and visualization of NPs. Unfortunately, none can differentiate the core and the shell of the NPs. Spectral imaging has been used to distinguish a drug molecule and its metabolite. We have recently integrated this technology to a resolution of 9 nm and by using artificial intelligence-driven analyses. Such resolution allowed us to collect much robust datapoints of each pixel of an image. Our analyses could recognize 45 spectral points within a pixel to detect unlabeled Ag-NPs and Au-NPs in single live cells and tissues (liver, heart, spleen and kidney). The improved resolution and software provided a more specific fingerprinting for each single molecule, allowing simultaneous analyses of 990 complex interactions from the 45 points for each molecule within a pixel of an image. This in turn allowed us to detect surface-functionalization of Ag-NPs to distinguish the core from the shell of Ag-NPs for the first time. Our studies were validated using various laborious and time-consuming conventional techniques. We propose that spectral imaging has a tremendous potential to study NP localization and identification in biological samples at a high temporal and spatial resolution, based primarily on the spectra identity information.

Introduction

The conventional methods used for the quantification of the inorganic NPs include inductively-coupled plasma mass spectrometry (ICP-MS) and inductively-coupled plasma atomic emission spectroscopy (ICP-AES)[1-3]. In addition to the matrix interference, some disadvantages in ICP-associated methods include chemical interference, the necessity of liquidized sample, low plasma sensitivity to organic solvents, and ineffectiveness of the nebulizer. Non-destructive techniques have also been developed. These include the use of fluorescent-labeled NPs[4, 5] and the modern ultrasonic holography[6, 7].

While fluorescent-conjugated NPs are generally used to identify NP localization in the live biological samples, such conjugation could interfere with NP function, localization, cytotoxicity and biodistribution[8-10]. Thus, different imaging modalities have been recently introduced to image unlabeled-NPs without destroying the biological tissues. Based on the light-refractive index of NPs, NPs detections in live cells have been performed[11]. The specific scattered-light of NPs allows real-time monitoring of unlabeled NPs[12]. In addition to Raman spectroscopy[13], a standard optical spectroscopic microscopy has also been used to image NPs, albeit this was done at a much narrow scanning range of 200 nm[14]. Different optical microscopy techniques to detect a specific spectrum of NPs have therefore been proposed to capture absorption spectra[15] and the plasmon resonance scattering or extinction spectra of various NPs[16-19].

Despite recent advances in optical microscopes, visualizing unlabeled-NPs remains a challenge. This is primarily due to the intensity-based measurements performed at a very narrow spectrum optimized for different studies and systems at different laboratories. We recently introduced a

spectral imaging in which broader spectral characteristics are first identified, characterized and stored in a library[20]. Unlike other previous studies, however, our current studies did not identify a molecule based merely on the spectral intensity, relative intensity, or spectral points. Our new strategies using a higher spectral resolution and artificial intelligence for point recognition improved our capability to differentiate two very similar molecules.

Results

We could now scan absorbance spectra from 400 nm to 800 nm with a resolution of 9 nm (**Supp Fig. 1**). This improved spectral imaging provides much detailed information for a more accurate image analysis, resulting in unique 45 spectral points for each pixel. These points are interconnected resulting in 990 unique interactions (**Supp Fig. 2**). Using artificial intelligence-driven analysis to recognize relative interactions between 2 points, the integrations of such interactions provide unique fingerprints for different chemicals. The key feature is that we could recall all these specific interactions from the library fairly quickly. These relative interaction points become the unique identity (or fingerprinting) of a molecule.

We report here that spectral imaging can provide a high temporal and spatial resolution of silver nanoparticles with shell (Ag(s)-NPs) or without shell (Ag-NPs). Our validation results on gold nanoparticles (Au-NPs) are located mainly in the supplements. These NPs were characterized for their syntheses, hydrodynamic sizes and structural compositions (**Supp Fig. 3; see Method**).

Spectra signatures of Ag(s)-NPs and Ag-NPs were identified with a major peak at 420 nm.

Using a microscope equipped with hyperspectral imaging (GenASIs from Applied Spectral Imaging), we imaged and recorded the spectral characteristics of the clusters of Ag(s)-NPs before and after incubated with the cells (**Fig. 1a**). We captured the spectral range between 400-800 nm for Ag(s) NPs in the present and absent of cells. Ag(s)-NPs had characteristics spectra with a distinctive peak at 420 nm (**Fig. 1b**). This peak was consistent with previous study[21]. While this peak was the main characteristic of Ag(s)-NPs, we also looked at different features that could contribute to the characteristic of Ag(s)-NPs. Interestingly, we could generate two distinct libraries

for Ag(s)-NPs. The peak of Ag(s)-NPs could be distinctively differentiated by the additional "shoulder" that only appeared at the peripheral or shell of the NPs. Of note, silver-polymer core-shell NPs are generally known for their unique optical properties, in which the shell of Ag also plays a critical role in protecting the Ag core[22, 23]. The shift in the shoulder peak could therefore be used to differentiate the core and shell of Ag-NPs clusters. We quantified the spectral intensities of these peaks before and after 18-hour incubation with cells (**Fig. 1c**). As verified with traditional spectrophotometry, the linearity of Ag(s)-NPs was observed at the peak of 420 nm (**Supp Fig. 4a**), indicating that we could predict the singularity or number of NPs in each pixel of an image based on the peak intensity of the spectra. Extrapolating from these intensity differences, our data suggested that Ag(s)-NPs tended to aggregate more in solution than in the cells (**Fig. 1d**).

To confirm our observation of Ag(s)-NPs, we synthesized the Ag-NPs exclusively without the shell. The spectral characteristics of the Ag-NPs before and after incubation with the cells were recorded (**Supp Fig. 5a**). Ag-NPs have the same characteristics spectra of Ag(s)-NPs, at ~420 nm, except that Ag-NPs spectra revealed without the additional "shoulder" (**Supp Fig. 5b**). We also calculated the spectral intensities of these peaks before and after 18-hour incubation with cells (**Supp Fig. 5c**). This disclosed the specificity of spectral imaging to differentiate between the spectral characteristics of different types of silver NPs (Ag-NPs and Ag(s)-NPs).

Spectra signature of Au-NPs was identified with a major peak at 552 nm.

Another inorganic NPs was prepared to further confirm the capabilities of spectral imaging to identify a different NP, Au-NPs (**Supp Fig. 6a**). Capturing spectra between 400-800 nm revealed that the Au-NPs had a unique spectra peak ranged between 520 and 580 nm (**Supp Fig. 6b**),

consistent with previous study[24]. Background spectra without or with cells were captured to differentiate spectral intensity at 552 nm peak (**Supp Fig. 6c**). The specific subcellular localization of Au-NPs in the cells could be determined by examining the spectral characteristics of each pixel in the image. In the fixed cells, after treated with Au-NPs for 18 hours, we could detect individuals or clusters of Au-NPs. To independently verify the microscopy spectra, we examined the Au-NPs spectra using traditional spectrophotometry (**Supp Fig. 4b**). The linearity of Au-NPs was observed at the peak of 536 nm, indicating that we could predict the singularity or number of NPs in each pixel of an image based on the peak intensity of the spectra. Extrapolating from these data, our studies suggested that Au-NPs tended to disperse more readily in the cells than in solution (**Supp Fig. 6d**).

Spectral imaging showed dynamics Ag(s)-NP or Au-NP accumulation in the cell nucleus.

Once the spectral signatures for both Ag(s)-NPs and Au-NPs were identified and defined in the libraries, analytical software was used to perform spectral identity for each pixel of an image in order to identify pixels with spectral resemblance of Ag(s)-NPs or Au-NPs. Background spectral could be taken from the non-treated cells (negative control) or different areas within the field of view in the image (**see Method**). This was a powerful method to trace non-fluorescence inorganic substances. We thus applied this technique on the time-lapse imaging of cells treated with 0.1 mg Ag(s)-NPs in 2 mL cell media (**Fig. 2a; Supp Fig. 7**). We observed the continuous accumulation of Ag(s)-NPs in the cells. Our libraries could distinctively differentiate the core (pink color) and shell (yellow color) clusters of Ag(s)-NPs. Once the pixel identity of Ag(s)-NP signature spectra was identified, we randomly selected a pixel to study individual spectra after background subtraction (**Fig. 2b; Supp Fig. 8**). We quantified spectra representing NPs in the cytoplasm or

nucleus within single cells (**Fig. 2c**). It was apparent that our Ag(s)-NPs were dynamically moving in and out of the cells, as depicted in the fluctuation in the total NPs in a single cell. The NPs were also moving in and out of the cell nucleus, as shown by the number of NPs in the nucleus at each time point. In this particular study, cells were also moving in or out from our field of view. More Ag(s)-NPs would eventually accumulate in the cells. Ag(s)-NPs would subsequently accumulate in the cell nucleus (**Supp Figs. 7 and 8**).

We next studied time-lapse imaging of Au-NPs in single living cells (**Supp Figs. 9a and 10**). We noted the continuous accumulation of Au-NPs in the cells. Once the pixel resembling Au-NP spectral signature was identified, we randomly selected a pixel to study individual spectra after background subtraction (**Supp Figs. 9b and 10**). Through the time-lapse imaging to detect the movements of Au-NPs, we could quantify potential NPs in the cytoplasm or nucleus within single cells (**Supp Fig. 9c**). It was apparent that Au-NPs were dynamically moving in and out of the cells, as indicated by the fluctuation in total NPs in a single cell at a single time point. Similarly, NPs were in and out of the cell nucleus as depicted by the number of NPs in the nucleus at each time point. As time passed, more NPs accumulated in the cells, but this accumulation was started from the cytoplasm and followed by the nucleus. It was evident that Au-NPs preferentially localized in the cell nucleus (**Supp Figs. 10 and 11**). While both Au-NPs and Ag(s)-NPs are largely known to localize in the nucleus[25, 26], we showed for the first time the dynamics movements of Au-NPs and Ag-NPs in cytosol and nucleus (**Supp Figs. 7 and 10**).

Electron microscopy and silver-staining were used to verify the spectral imaging approach.

To verify our subcellular localization findings of NPs in time-lapse imaging studies, we performed transmission electron microscopy (TEM) and silver staining analyses. The TEM captured images cells treated with Ag(s)-NPs, Ag-NPs, and Au-NPs for 16 hours (**Fig. 3a; Supp Fig. 12a**). While we were not able to capture the dynamics of these NPs due to the sample fixation, the TEM studies confirmed the accumulation of NPs in the cell nucleus. Likewise, the localization of NPs was confirmed to be mostly in the nucleus of cells using a silver staining to generate darker brown contrast in phase images (**Fig 3b; Supp Fig. 12b**). Because the contrast was primarily enhanced by metallic silver attached at the peripheral of the NPs, the spectral signatures within the NPs were not much altered (**Fig 3c; Supp Fig. 12c**).

Verification of spectral imaging approach was performed *in vivo* using ICP-MS.

We next assessed the practicality of spectral imaging to study the distribution of the NPs within mouse organ tissues. Remarkably, we found that distributions of the Ag(s)-NPs, Ag-NPs and Au-NPs in kidney, spleen, liver and heart tissues (**Fig. 4a, Supp Figs. 13 and 14**). Importantly, the spectral characteristics of the core and shells of Ag(s)-NPs were not altered (**Fig. 4b,c**). Based on our quantitative analyses, we showed that Ag(s)-NPs and Ag-NPs were distributed highly in kidney and spleen, respectively (**Fig. 5a**). On the other hand, Au-NPs were in the liver (**Supp Fig. 15a**). As a validation of the NPs distribution within the organs, we conducted ICP-MS analyses. Of note, ICP-MS method and its standard curve did not differentiate between Ag(s)-NPs and Ag-NPs (**Supp Fig. 15b**). We performed separate analyses of those tissues for Ag(s)-NPs, Ag-NPs or Au-NPs (**Fig. 5b, Supp Fig. 15c**). We next examined the correlation analyses of the NPs distribution. We found a significant correlation in Ag(s)-NPs and Ag-NPs distributions in spectral imaging and ICP-MS among the tissues (**Fig. 5c**). Likewise, a similar correlation was observed in

Au-NPs (**Supp Fig. 15d**), indicating a consistency between spectral imaging and ICP-MS approaches.

Discussion

The significance of the use of spectral imaging in our studies are as follows. *First*, we were able to identify and quantify the presence of NPs without the need to destruct or liquify the samples. This allowed us to perform live-cell imaging that was otherwise not possible. *Second*, we could calibrate the spectra library by using both imaging and the singularity/plurality of spectra "signature" of a chemical. In Ag(s)-NPs, for example, we could pick up the plurality of spectra at the 420 nm, i.e. peak with or without a shoulder. Looking at the images, we showed that the peaks without shoulder were always at the center of NPs, whereas the peaks with a shoulder were localized at the peripheral. *Third*, we did not need to label our NPs with fluorescent. Labeling NPs required an additional step in the synthesis process, making the process more expensive and laborious. Labeled NPs could also alter the molecular functions and characteristics of NPs[8-10]. *Fourth*, spectral imaging was also applicable to fluorescent or auto-fluorescent molecules. Using spectral imaging, we were able to perform fluorescent molecules fairly easily based mainly on its predominant fluorescence spectra (data not shown)[20]. Note that the spectral identities might be different between non-labeled and fluorescent-labeled NPs. A fluorescence microscopy might be more practical to detect the fluorescent-labeled NPs. *Fifth*, the spectral imaging approach was a simple yet inexpensive method for unlabeled NPs, resolution of which was depended on the quality of lens and camera from standard optical microscopes. Unlike laser-based microscopic devices, such as Raman spectroscopy, spectral imaging systems could be installed on upright or inverted microscopes that were readily available in many research laboratories.

Using spectral imaging, we were able to observe the dynamic uptake, movement, and distribution of different types of free-labeled NPs in single cell. Conducting the live imaging technique with

scanning the spectra from 400-800 nm, we were able to instigate the behaviors of the NPs in single cell, in which the NPs were eventually accumulate in the cell nucleus. The spectral imaging was validated by both TEM and silver staining studies, although TEM and silver staining techniques did not provide live-dynamics nature of NPs due to the requirement for cell fixation. In addition, we were able to study the distribution of NPs among tissue using the spectral imaging. We found that Ag(s)-NPs and Ag-NPs were primarily localized in kidney and spleen, respectively. On the other hand, Au-NPs were distributed primarily in the liver. Of note, these tissues could be easily visualized with a standard H&E staining, allowing easier sample preparation relative to the ICP-MS approach. It is known that larger nanoparticles (> 6 nm) are cleared from the blood by the reticuloendothelial system. They accumulate in the liver and spleen; they are also captured by the mononuclear phagocyte system, which can be eliminated by the hepatobiliary system or may remain in the body for a long time[27-29]. However, it has been reported that the highest concentration of Ag-NPs is initially found in the liver, and over time the highest concentration of Ag-NPs should be found in the spleen[30]. Importantly, the spectral imaging was confirmed by the conventional ICP-MS technique with regards to tissue distribution analyses.

A few label-free methods have been produced for observing NPs in live cells. For examples, transitory absorption microscopy has been utilized to capture carbon nanotubes in cells, and scatter-enhanced phase-contrast microscopy has been utilized to assess the intracellular behavior of unlabeled silicon nanowires[15, 31]. Other approaches such as hyperspectral stimulated Raman scattering microscopy[13], optical diffraction tomography[11], and dark-filed microscopy[32], have been utilized to investigate unlabeled NPs inside cells. However, using current technology to track unlabeled NPs in live cells in real-time with reliable spatial resolution remains a challenge.

Besides, it is necessary to monitor both NPs and biomolecules to fully comprehend the interaction between NPs and cells/tissues. To the best of our knowledge, no technique has utilized a broader band of spectra 400-800 for real-time imaging in label-free NPs. The broader spectra is required to extract more precise characteristics of a single molecule[20]. Specifically, this approach provides a more specific fingerprinting for each NPs.

In summary, the combination of spectroscopy and imaging provide high-resolution spatial and temporal information of spectra characteristics in each pixel. This approach could serve as a valuable technique to understand distribution, dynamic movement, and behavior of nanoparticles used in biomedical research and clinical medicine.

Conclusions

Spectral imaging provides both intensity and spectral information for each pixel of an image. We have achieved spectra resolution to 9 nm between 400-800 nm, resulting in 45 unique datapoints for each spectrum in each pixel. We have also integrated our image and spectral analyses by using artificial intelligence to recognize the datapoints by interconnecting each point to provide a unique information of chemical fingerprints. This strategy allows differentiation between the core from the shell of silver-nanoparticles (Ag-NPs) for the first time. The advances of spectral imaging resolution and analysis also allow us to detect the dynamics of NPs distribution and tracking/identifying NPs and their subcellular localizations in single living cells. Without labeling the NPs and destroying the samples, the advanced spectral microscopy technique allows analyzing NPs in fixed cells, living cells and tissue samples *in vivo*.

Acknowledgments. This work was supported in part by the NIH HL131577 and HL131577-S1. The authors acknowledge the use of facilities and instrumentation at the UC Irvine Materials Research Institute (IMRI), which is supported in part by the National Science Foundation through the UC Irvine Materials Research Science and Engineering Center (DMR-2011967). The completion of this work by QAA partially fulfilled the requirements for her Ph.D. degree program in Biomedical and Pharmaceutical Sciences. At Chapman University, A Sharma provided advices on the imaging validations, F Amirrad assisted QAA in the supervising the tissue processing training, M Takahashi and D Larin-Henriquez were involved in mouse maintenance, reagent preparations and ordering. Li Xing at IMRI assisted in TEM studies.

Author Contributions. QAA collected data, analyzed data and drafted the manuscript. RP and AKB synthesized and characterized the nanoparticles and helped design some studies. SOA contributed in the H&E and silver staining experiments (double-blind). AMN provided data, statistical analyses and improved interaction points in the software. NK participated in the spectral imaging system and software analysis. AMM analyzed the TEM images. SMN conceived the idea, designed research and oversaw the experimental progress. All authors were participating in finalizing the draft of the manuscript.

Conflicts of Interest. None

Declaration. All animal procedures were performed in accordance with the Guidelines for Care and Use of Laboratory Animals of Chapman University. The Institutional Animal Care and Use Committee at Chapman University approved our animal studies, and our animal facility was approved by the Office of Office of Laboratory Animal Welfare (OLAW). The OLAW assurance number is D17-00960.

References

1. D. C. Antonio, C. Cascio, D. Gilliland, A. J. Nogueira, F. Rossi and L. Calzolai, *Biointerphases*, 2016, **11**, 04B309.
2. D. Vanhecke, L. Rodriguez-Lorenzo, M. J. Clift, F. Blank, A. Petri-Fink and B. Rothen-Rutishauser, *Nanomedicine (Lond)*, 2014, **9**, 1885-1900.
3. S. Lee, X. Bi, R. B. Reed, J. F. Ranville, P. Herckes and P. Westerhoff, *Environ Sci Technol*, 2014, **48**, 10291-10300.
4. R. Pala, A. M. Mohieldin, R. T. Sherpa, S. H. Kathem, K. Shamloo, Z. Luan, J. Zhou, J. G. Zheng, A. Ahsan and S. M. Nauli, *ACS Nano*, 2019, **13**, 3555-3572.
5. R. Pala, A. M. Mohieldin, K. Shamloo, R. T. Sherpa, S. H. Kathem, J. Zhou, Z. Luan, J. G. Zheng, A. Ahsan and S. M. Nauli, *Nano Lett*, 2019, **19**, 904-914.
6. G. S. Shekhawat and V. P. Dravid, *Science*, 2005, **310**, 89-92.
7. L. Tetard, A. Passian, K. T. Venmar, R. M. Lynch, B. H. Voy, G. Shekhawat, V. P. Dravid and T. Thundat, *Nat Nanotechnol*, 2008, **3**, 501-505.
8. S. Snipstad, S. Hak, H. Baghirov, E. Sulheim, Y. Morch, S. Lelu, E. von Haartman, M. Back, K. P. R. Nilsson, A. S. Klymchenko, C. de Lange Davies and A. K. O. Aslund, *Cytometry A*, 2017, **91**, 760-766.
9. T. Tenuta, M. P. Monopoli, J. Kim, A. Salvati, K. A. Dawson, P. Sandin and I. Lynch, *PLoS One*, 2011, **6**, e25556.
10. C. Corbo, R. Molinaro, A. Parodi, N. E. Toledano Furman, F. Salvatore and E. Tasciotti, *Nanomedicine (Lond)*, 2016, **11**, 81-100.
11. D. Kim, N. Oh, K. Kim, S. Lee, C. G. Pack, J. H. Park and Y. Park, *Methods*, 2018, **136**, 160-167.
12. F. Wang, B. Chen, B. Yan, Y. Yin, L. Hu, Y. Liang, M. Song and G. Jiang, *J Am Chem Soc*, 2019, **141**, 14043-14047.
13. B. Huang, S. Yan, L. Xiao, R. Ji, L. Yang, A. J. Miao and P. Wang, *Small*, 2018, **14**.
14. G. L. C. Spicer, L. Almassalha, I. A. Martinez, R. Ellis, J. E. Chandler, S. Gladstein, D. Zhang, T. Q. Nguyen, S. Feder, H. Subramanian, R. de la Rica, S. A. Thompson and V. Backman, *Nanoscale*, 2018, **10**, 19125-19130.
15. J. F. Zimmerman, R. Parameswaran, G. Murray, Y. Wang, M. Burke and B. Tian, *Sci Adv*, 2016, **2**, e1601039.
16. L. Q. Chen, L. Fang, J. Ling, C. Z. Ding, B. Kang and C. Z. Huang, *Chem Res Toxicol*, 2015, **28**, 501-509.
17. S. Patskovsky, E. Bergeron, D. Rioux and M. Meunier, *J Biophotonics*, 2015, **8**, 401-407.
18. L. Q. Chen, S. J. Xiao, L. Peng, T. Wu, J. Ling, Y. F. Li and C. Z. Huang, *J Phys Chem B*, 2010, **114**, 3655-3659.
19. J. Ling, Y. F. Li and C. Z. Huang, *Anal Chem*, 2009, **81**, 1707-1714.
20. Q. A. Alshammari, R. Pala, N. Katzir and S. M. Nauli, *Sci Rep*, 2021, **11**, 2703.
21. A. M. Fayaz, K. Balaji, M. Girilal, R. Yadav, P. T. Kalaichelvan and R. Venketesan, *Nanomedicine*, 2010, **6**, 103-109.
22. N. Claes, R. Asapu, N. Blommaerts, S. W. Verbruggen, S. Lenaerts and S. Bals, *Nanoscale*, 2018, **10**, 9186-9191.
23. E. Ertem, B. Gutt, F. Zuber, S. Allegri, B. Le Ouay, S. Mefti, K. Formentin, F. Stellacci and Q. Ren, *ACS Appl Mater Interfaces*, 2017, **9**, 34762-34772.

24. W. Haiss, N. T. Thanh, J. Aveyard and D. G. Fernig, *Anal Chem*, 2007, **79**, 4215-4221.
25. R. I. Berbeco, H. Korideck, W. Ngwa, R. Kumar, J. Patel, S. Sridhar, S. Johnson, B. D. Price, A. Kimmelman and G. M. Makrigiorgos, *Radiat Res*, 2012, **178**, 604-608.
26. P. V. Asharani, M. P. Hande and S. Valiyaveettil, *BMC Cell Biol*, 2009, **10**, 65.
27. Y. N. Zhang, W. Poon, A. J. Tavares, I. D. McGilvray and W. C. W. Chan, *J Control Release*, 2016, **240**, 332-348.
28. A. M. Alkilany and C. J. Murphy, *J Nanopart Res*, 2010, **12**, 2313-2333.
29. M. Longmire, P. L. Choyke and H. Kobayashi, *Nanomedicine (Lond)*, 2008, **3**, 703-717.
30. K. Dziendzikowska, J. Gromadzka-Ostrowska, A. Lankoff, M. Oczkowski, A. Krawczynska, J. Chwastowska, M. Sadowska-Bratek, E. Chajduk, M. Wojewodzka, M. Dusinska and M. Kruszewski, *J Appl Toxicol*, 2012, **32**, 920-928.
31. L. Tong, Y. Liu, B. D. Dolash, Y. Jung, M. N. Slipchenko, D. E. Bergstrom and J. X. Cheng, *Nat Nanotechnol*, 2011, **7**, 56-61.
32. E. A. Gibbs-Flournoy, P. A. Bromberg, T. P. Hofer, J. M. Samet and R. M. Zucker, *Part Fibre Toxicol*, 2011, **8**, 2.

Figure 1

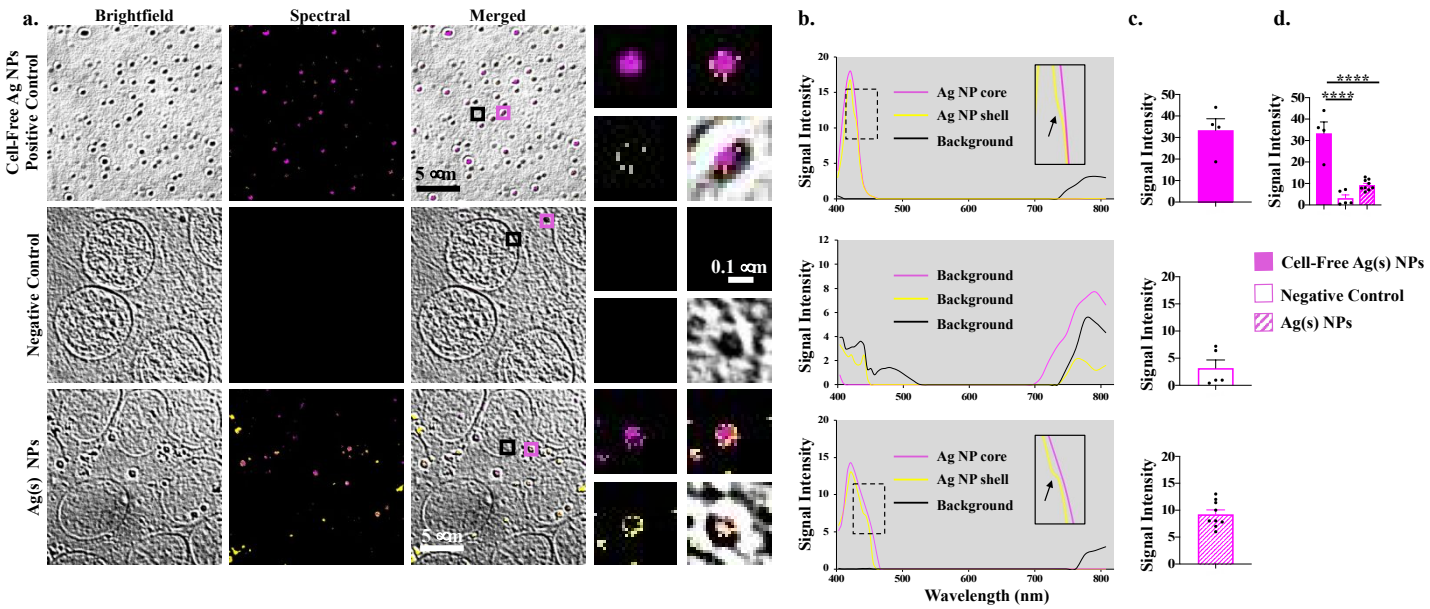

Figure 1. Identification of Ag(s)-NPs spectra
(a) Brightfield images of the Ag(s)-NPs in the cell-free system (positive control), fixed cells (negative control), and 16-hour Ag(s)-NPs-treated cells (Ag(s)-NPs) were captured. The spectral images were extracted from the spectra library for the Ag(s)-NPs. Merged images illustrate superimposed brightfield and spectral images. The pink spectral image exhibits the core area of the Ag(s)-NPs cluster, while the yellow color represents the shell region. **(b)** The graphs illustrate the wavelength peaks at ~420 nm for the positive control and the incubated cells. The pink wavelength displays the intensity of the core area; the yellow wavelength shows the shell part (with a small shoulder; insert and arrow). The black color exhibits the spectrum of the background area. The negative control spectra were identified based on unmatched spectra from our libraries. **(c)** The bar graphs show the variation of intensity data points at 420 nm. **(d)** The signal intensities were compared among cell-free positive control, non-treated cells negative control, and Ag(s)-NPs-treated cells. N=4-5 for each positive and negative controls; N=8 for experimental groups. ****, P<0.0001.

Figure 2

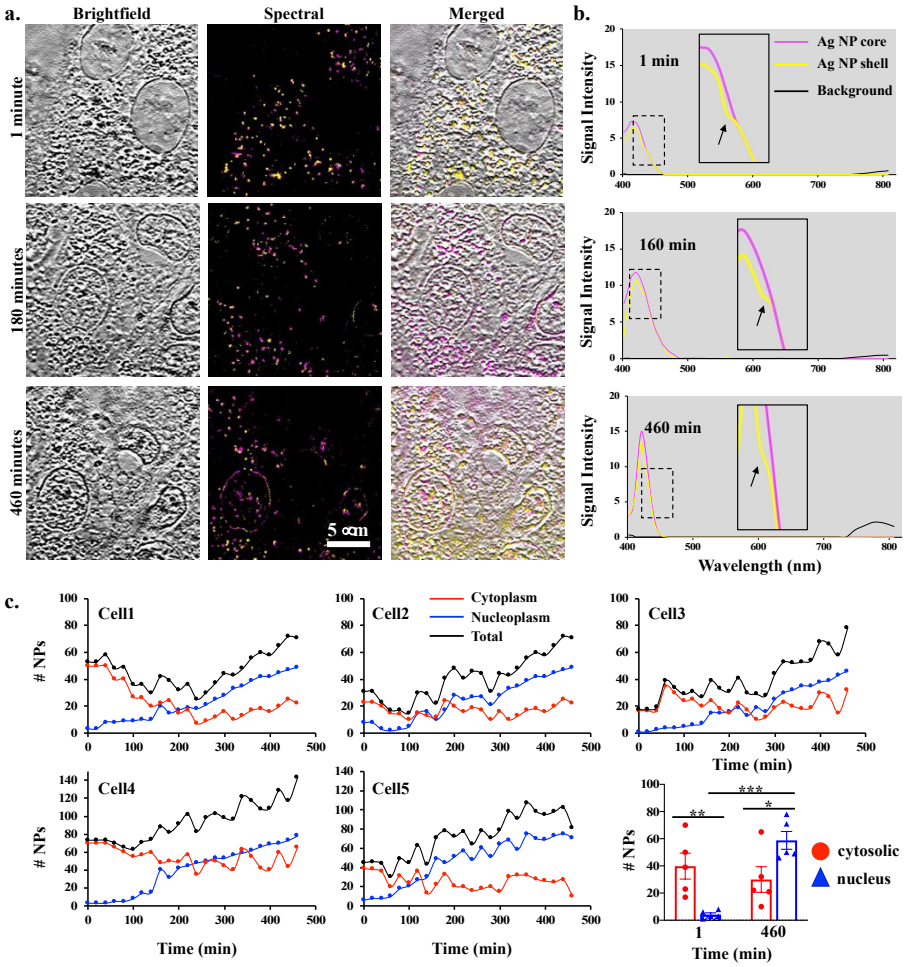

Figure 2. Time-lapse imaging of Ag(s)-NPs
(a) Sequential time imaging of cells treated with 0.1 mg of Ag(s)-NPs in 2 mL media was captured for about 8 hours. Brightfield images and spectral scans were taken every 20 minutes (**Supp Fig. 4**). **(b)** Spectral analysis was performed at the end of 8 hours after subtraction from the background spectra (**Supp Fig. 5**). The Ag(s)-NPs libraries differentiated the core and shell of NP clusters. The pink wavelength displays the intensity of the core area; the yellow wavelength shows the shell part (with a small shoulder; insert and arrow). **(c)** Line graphs illustrate the time-lapse analysis from 5 independent experiments. A number of Ag(s)-NPs (#NPs) was measured in one cell at each time point. Total #NPs were calculated from localization NPs in the cytoplasm (outside the nucleus) and nucleoplasm (inside the nucleus) within a cell. Comparisons were made at the beginning (1 min) and end (460 min) of the 8-hour experiments. N=5. *, P<0.05; **, P<0.01; ***, P<0.001.

Figure 3

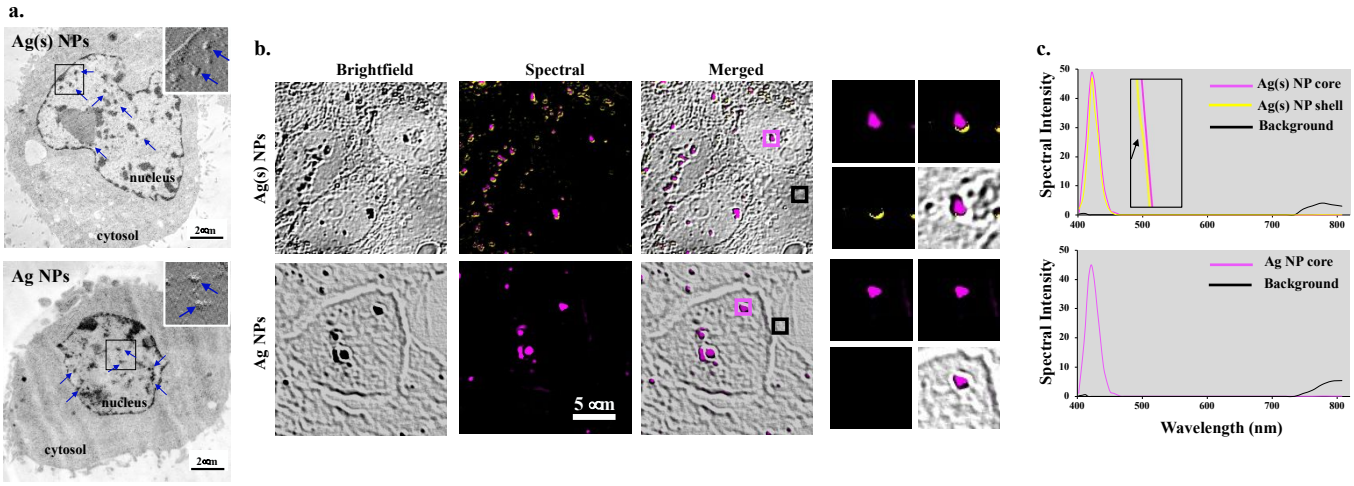

Figure 3. TEM & Silver staining of Ag(s)-NPs and Ag-NPs
(a) TEM analyses were performed after treatment of Ag(s)-NPs or Ag-NPs for 16 hours. An embossing filter was applied in some regions of cell nucleus for better clarity of the presence of NPs (insert with arrows). **(b)** Cells after silver staining show brightfield images of the Ag(s)-NPs and Ag-NPs treated cells for 16 hours. The spectral images were extracted and pseudo-colored for the Ag(s)/Ag-NPs. Merged images revealed superimposed brightfield and spectral images to show the location of Ag(s)/Ag-NPs in the cell nucleus. The pink pseudocolor shows the core area of the Ag(s)/Ag-NPs, while the yellow color represents the shell region of Ag(s)-NPs. **(c)** The spectral graphs clarify the wavelength peaks of Ag(s)/Ag-NPs at ~420 nm. The pink wavelength exhibits the intensity of the core area; the yellow wavelength displays the shell region. The black color shows the spectrum of the background area. N=5.

Figure 4

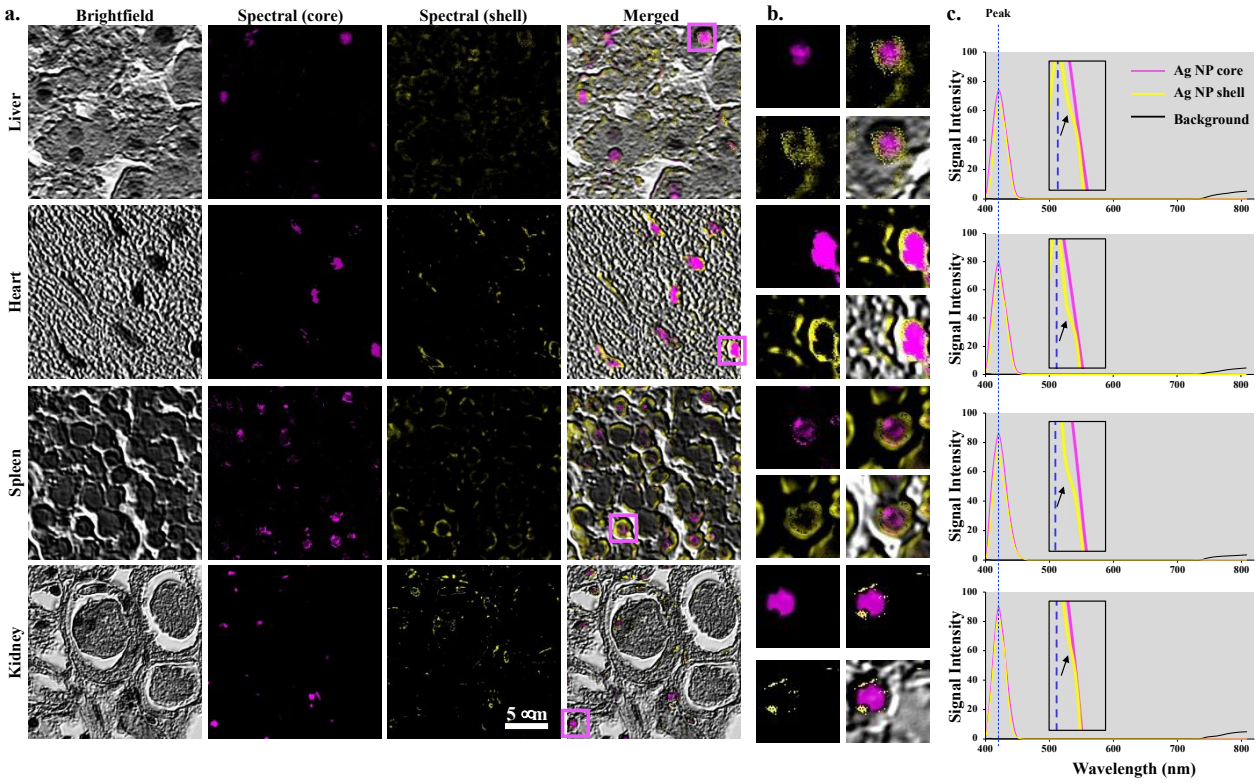

Figure 4. Distribution of Ag(s)-NPs in animal tissues
(a) Brightfield images of the Ag(s)-NPs at different organs tissues (liver, heart, spleen kidney) after intravenous injection with Ag(s)-NPs for 24 hours are shown. The spectral images were extracted from the spectra libraries for Ag(s)-NPs. Merged images display combined brightfield and spectral images. **(b)** The pink pseudo-colored images show the core area of the Ag(s)-NPs, while the yellow color exemplifies the shell region. **(c)** The graphs reveal the wavelength characteristics of the Ag(s)-NPs cluster at ~420 nm. The pink wavelength exhibits the intensity of the core area; the yellow wavelength displays the shell part. The background is shown as a black color wavelength. N=5.

Figure 5

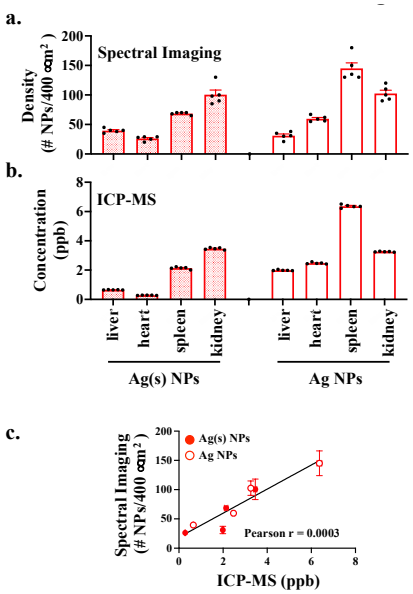

Figure 5. Correlation analysis of Ag(s)-NP and Ag-NP distributions in the tissues using spectral imaging and ICP-MS

The bar graphs exhibit the distributions of Ag(s)-NPs and Ag-NPs in liver, heart, spleen, kidney, which were done performed using spectral imaging **(a)** or ICP-MS **(b)**. **(c)** The correlation analysis of the distribution of Ag(s)-NPs and Ag-NPs in different organs between ICP-MS and spectral imaging is shown. N = 5 for each group and organs.